DOI: 10.48011/sbse.v1i1.2440

Computation of Transient Voltages on the Interconnected Grounding Grids ⋆

Walter Luiz Manzi de Azevedo *
Anderson Ricardo Justo de Araújo ** **José Pissolato Filho** ***

* *School of Electrical and Computer Engineering, University of Campinas, Campinas, São Paulo, Brazil (e-mail: w157573@dac.unicamp.br)*
** *School of Electrical and Computer Engineering, University of Campinas, Campinas, São Paulo, Brazil (e-mail: ajusto@dsce.fee.unicamp.br)*
*** *School of Electrical and Computer Engineering, University of Campinas, Campinas, São Paulo, Brazil (e-mail: pisso@dsce.fee.unicamp.br)*

Abstract: Grounding grids play a fundamental role to provide safety during electromagnetic transients and reliable operation of any electrical system under normal conditions. In this context, when lightning strikes a transmission line, surge currents will propagate to the electrical substations where grounding grids must dissipate these impulsive currents into the soil. Grounding grids are composed of horizontal bars welded with vertical forming a large mesh. Additionally, the interconnected grids are largely employed to guarantee safety for personnel and equipment in facilities. Due to several natural conditions, horizontal bars can be damaged and compromise the performance of the grounding grid in power plants. In this paper, transient voltages are computed for whole and damaged grids when lightning strikes a transmission line. Results have shown that there is a difference in the transient voltage peaks in these two conditions. To decrease these voltages, vertical rods are installed in the border of the grounding grids, which has been shown as an effective solution to lower these voltage peaks in the damaged grounding grids.

Resumo: Malhas de aterramento são fundamentais para fornecer segurança durante transitórios eletromagnéticos e uma operação confiável de sistemas elétricos em condições normais. Nesse contexto, quando uma descarga atmosférica atinge uma linha de transmissão, correntes impulsivas se propagam em direção à subestação elétrica onde malhas de aterramento devem dissipar esses surtos para o solo. Malhas de aterramento são compostas por eletrodos horizontais soldados com hastes verticais formando uma grande reticulado. Além disso, malhas interconectadas são empregadas para garantir a segurança de pessoas e equipamentos em instalações industriais. Devido às diversas condições naturais, os eletrodos horizontais podem se danificar e comprometer a performance da malha de aterramento. Neste artigo, as tensões transitórias são computadas para uma malha íntegra e outra danificada, submetidas à uma descarga atmosférica incidente em uma linha aérea. Os resultados mostram que existe uma diferença nos picos das tensões transitórias nessas duas condições. Para reduzir as tensões transitórias, hastes verticais são instaladas na borda da malha de aterramento, o que mostrou ser uma solução efetiva para diminuir esses picos de tensão em malhas danificadas.

Keywords: lightning discharges; transient voltages; grounding grid; grounding electrodes
Palavra-chaves: descargas atmoféricas, tensões transitórias, malhas de aterramento; eletrodos de aterramento

1. INTRODUCTION

Grounding systems must provide safety during electromagnetic transients and reliable operation of any electrical system under normal conditions. In a power substation, grounding grids must provide a low impedance path to dissipate surge currents into earth, generated by lightning strikes or by faults in which may exceed safety limits to personnel in the vicinity and to equipment installed in the facilities Harrat et al. (2011).

The touch and step voltage are important parameters during the grounding grid design that must provide safe values to prevent hazardous shocks to humans Otero et al. (2000). In order to obtain effectively a low grid impedance, several researchers have developed different models based on analytical formulae, lumped or distributed circuit mod-

⋆ This work was supported by São Paulo Research Foundation (FAPESP) (grant: 2019/01396-1)

els and electromagnetic field approaches Jardines et al. (2014); Grcev and Heimbach (1997).

Grounding grids consist of a combination of vertical bare copper rods welded with horizontal conductors at the cross-connections buried below the ground surface, occupying a considerable area. Additionally, interconnected grounding grids are employed for protection of workers in the oil and gas industrial plants face the risk of fire and explosions that may be caused by lightning strikes in the vicinity. Then, well-designed interconnected grounding grids must guarantee the safety limits Hassan et al. (2012); Ala et al. (2018). Due to several natural phenomena, such as soil salinity, freezing, corrosion and electromotive forces between conductors, the grounding bars may be damaged in the arrangement and this defect will impact the performance and the protection provided by the grounding grid which compromises the power system operation and the safety of the workers Chikarov et al. (2014); Wang et al. (2019).

In this paper, transient voltages are computed for whole and damaged interconnected grounding grids when lightning strikes at the transmission line. Results have show a significant difference for the transient voltage peaks in these two conditions. An alternative to overcome these high peaks are the installation of vertical rods in the border of the grounding grids, which has been shown as effective solution to lessen the transient voltages in the interconnected grounding grids.

2. GROUNDING GRID MODELLING

To compute the transient responses on grounding grids, several approaches have been proposed in the literature to model the vertical and horizontal conductors, based on: (i) lumped circuit Grcev and Popov (2005) (ii) transmission line theory Jardines et al. (2014) and (iii) electromagnetic field Sheshyekani et al. (2009). In this work, it is adopted the lumped circuit approach to represent the whole substation grounding mesh formed by horizontal electrodes arranged in squares with four earthing rods placed downside at each corner of the foundation, as shown in Fig. 1Farkoush et al. (2019).

In Fig.1, h is the burial depth of the grounding system, L is the total square length. The electric parameters of soil, considering that they are frequency-independent, are: μ_S is the magnetic permeability, ε_s is the relative permittivity and ρ_s is the resistivity. The vertical rods and the equivalent circuit are depicted at Fig.2a-b.

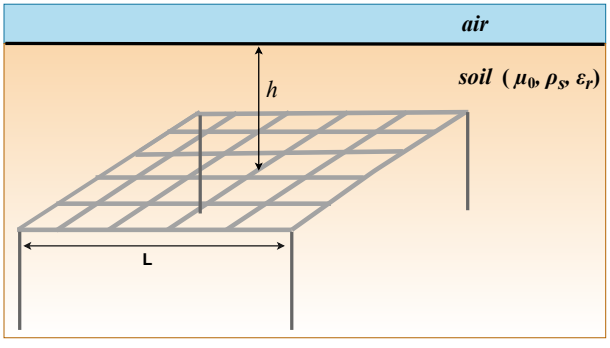

Figure 1. Generic grounding grid buried in a given soil.

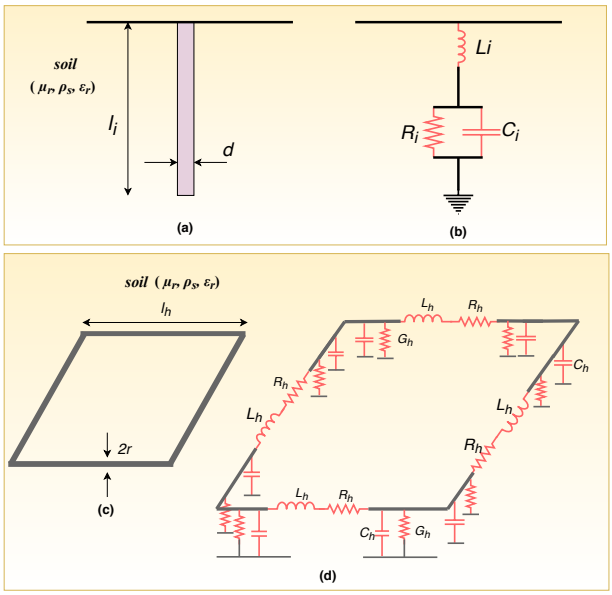

Figure 2. Modelling of the electrodes: [(a) Vertical rod and (b) its equivalent circuit; (c) Bar-cell and (d) its equivalent lumped circuit].

The electrical parameters for the vertical rod are given by Salam and Rahman (2016)

$$R_i = \frac{\rho_s}{2\pi l_i}\left[ln\left(\frac{8l_i}{d}\right) - 1\right]; \quad L_i = \frac{\mu_s}{2\,\pi}\, l_i ln\left(\frac{4l_i}{d}\right); \quad C_i = \frac{\epsilon_r l_i}{18\, ln\left(\frac{4l_i}{d}\right)} \times 10^{-9} \tag{1}$$

where d is the diameter of the vertical rod, l_i is the rod length and μ_s is the magnetic permeability of the soil ($\mu_s \approx \mu_0$). Based on the lumped circuit approach, the horizontal electrodes of the bar-cells can be represented by N sections of π-circuits in cascade, as illustrated in Fig.2c-d. The distributed parameters, in per-unit-length (p.u.l.) of the horizontal electrode are given by Han et al. (2011):

$$R'_h = \frac{\rho_c}{\pi a^2}; \quad L'_h = \frac{\mu_s}{2\pi}\left[ln\left(\frac{l_h}{a}\right) - 1\right]; \quad G'_h = \frac{2\pi}{\rho}\frac{1}{\left[ln\frac{l_h^2}{2ha} - 0.61\right]}; \quad C'_h = \epsilon_r \rho_s G'_h \tag{2}$$

where ρ_c is the conductor resistivity (copper), l_h is horizontal electrode length, a is the radius of the transversal section. The lumped parameters for π-circuit representation are given byGrcev and Grceva (2009); Sheshyekani et al. (2009):

$$R_h = R'_h\frac{l_h}{N}; L_h = L'_h\frac{l_h}{N}; C_h = C'_h\frac{l_h}{N}; G_h = G'_h\frac{l_h}{N} \tag{3}$$

Once the vertical and horizontal electrode are represented by the lumped parameters, the interconnected grounding grids can be formed and the transient voltages can be computed at several points, as describes in the next section.

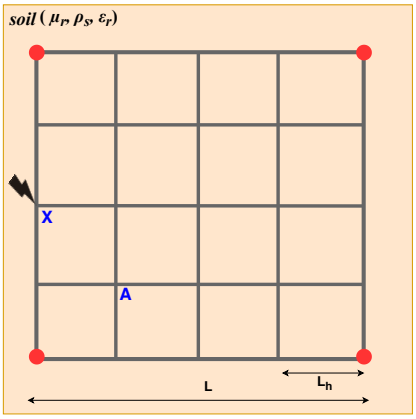

Figure 3. Top view of the single grounding grid studied.

Table 1. Data of the grounding grid.

Electrode	
horizontal	vertical
$\rho_c = 17.24$ nΩm	$d = 16$ mm
$l_h = 3$m	$l_i = 3$ m
$a = 7$ mm	$\rho_s = 1{,}000$ Ωm
$h = 0.5$ m	$\varepsilon_r = 10$

3. NUMERICAL RESULTS

This section is organized as follows: In sub-section 3.1, a comparison for grounding grid represented by the lumped parameters is performed. In sub-section 3.2, the transient voltages at several points for whole and damaged grounding grids are computed. Finally, in sub-section 3.3, vertical rods are appended at the interconnected grounding grid in order to reduce these transient voltages.

3.1 Validation of lumped representation of grounding grids

In order to validate the lumped model presented, simulation results of a single grounding grid hit by lightning strike are compared with those obtained by simulations results computed by the Numerical Inverse Laplace Transform (NILT) Ramirez et al. (2004). The single grounding grid is depicted at Fig.3.

In Fig.3, the grounding grid is 12×12m large ($L_T = 12$ m), where each bar-cell is 3×3 m ($L_h = 3$ m). Considering the maximum frequency of 1 MHz, and the soil parameters in Table 1, the critic length is 7.668 m Cecconi et al. (2005). Each side of the bar-cell is modelled by 1 π/m which satisfies the condition presented in Cecconi et al. (2005). The 4 vertical rods are represented by the circuit in Fig.2b and they are highlighted in red dots in the grid. The data of the grounding grid are in Table 1. The electric parameters of the horizontal and vertical electrodes are presented in Table 2. The lightning current is modelled by impulsive source given by a 1.20/50 μs double exponential function, as follows:

$$I(t) = I_0(e^{-at} - e^{-\beta t}) \tag{4}$$

where $I_0 = 1.037$ kA, $\alpha = 1.471 \times 10^4$ s^{-1} and $\beta = 2.471 \times 10^6$ s^{-1}, striking at the point X.

Table 2. P.u.l. Parameters of the horizontal and vertical electrodes.

Electrode			
horizontal (p.u.l.)		vertical	
$R'_h =$	0.11 mΩ/m	$R_i =$	380 Ω
$L'_h =$	0.931 μH/m	$L_i =$	4.47 μ
$C'_h =$	0.112 nF/m	$C_i =$	0.224 nF
$G'_h =$	1.30 mS/m	-	-

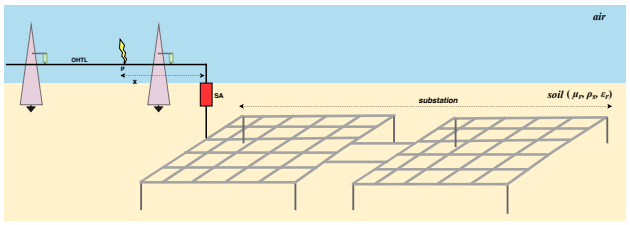

Figure 4. Schematic of the lightning discharge into a OHTL and the interconnected grounding grids in the substation.

In this paper, the lumped representation is chosen due to facility in the computation of the transient voltages at several points of the whole and damage grounding grids simulated in ATP software.

3.2 Transient Voltages at the interconnected grounding grids

In order to investigate the transient voltages at interconnected grounding grids, a simplified power system is employed for these simulations as illustrated in Fig.4. In this case, a overhead transmission line (OHTL) connects the generators to the electrical substation. The OHTL parameters are presented in Table 3.

A simplified transmission system is employed to compute the node transient voltages with a interconnected grounding grid incorporated in ATP. The same impulsive current was used to analyze the transient voltages of the interconnected grounding grids, as shown in Fig.4. The lightning strikes on the OHTL ($Z_c \approx 415$ Ω) at point P ($x = 10$ km) from the substation where a surge arrester SA is at the entrance, as illustrated in Fig. 4. The OHTL parameters are shown in Table 3, which are considered constants for all frequency-range. The OHTL is modelled by the *distributed parameters model-LINEZT* in ATP. For all the simulations, the soil is considered homogeneous, the electrical parameters of the soil (ρ and ε) are frequency-independent and ionization effect is not taken into account. The interconnected grounding grid configuration is depicted at Fig.5. The velocity of the surge current waves is given by:

$$v = \frac{1}{\sqrt{LC}} \tag{5}$$

Table 3. Parameters of the OHTL employed.

OHTL Parameters		
$R = 0.068\Omega$/km	$L = 1.80$ mH/km	$C = 10.369$ nF/km

Using the values of C and L in table 3, the velocity computed is $v \approx 0.77c$, where c is the speed of light ($c = 3 \times 10^5$ km/s). The travelling time τ is given by:

$$\tau = \frac{x}{v} = x\sqrt{LC} \tag{6}$$

Using the OHTL parameters of table 3, the traveling time is $\tau = 43.2$ μs, which will be used as time reference in the transient analysis. In order to compute the transient voltages, two scenarios were tested, described as follows:

- (S_1)-the interconnected grounding grid is in its complete state, with all integrated welded bar-cells and rods (designed by W in this work), under normal operation;
- (S_2)-the second mesh of the interconnected system presents a subtracted bar-cell at the bottom left corner (designed by D in this work), as highlighted in red bars at Fig.5.

The distance between the interconnected grounding grids is $L_T = 10$ m, $L = 12$ m and the previous horizontal and vertical parameters are employed in Fig.5. Considering a failure in the SA, the surge currents are injected directly in the grounding grid. The injected currents and voltage at the injection point for the whole grounding system are depicted in Fig.6.

It can be noted that after a traveling time τ, the current surge arrives at the injection point X, with the amplitude slight mitigated, due to the line losses. The transient voltage steeply increases to 4.20 kV at point X, which is the potential rise at the injection node. The transient voltages

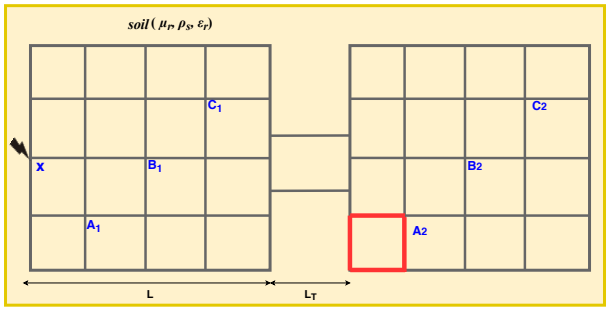

Figure 5. Top view of the interconnected grounding grid (GG) in the substation (red square is subtracted for the damaged GG).

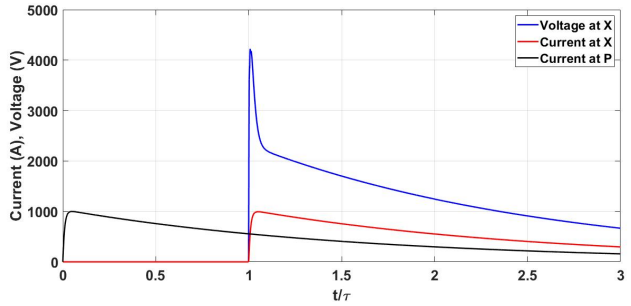

Figure 6. Injected current at OHTL (black line); Injected current at point X (red) and GPR at point X (blue).

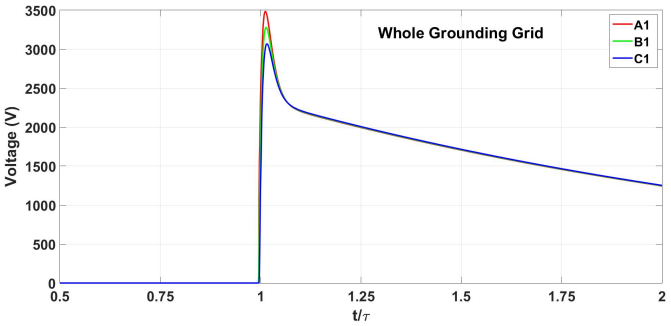

Figure 7. Voltages at the points A_1, B_1 and C_1 for a whole integrated grounding grid.

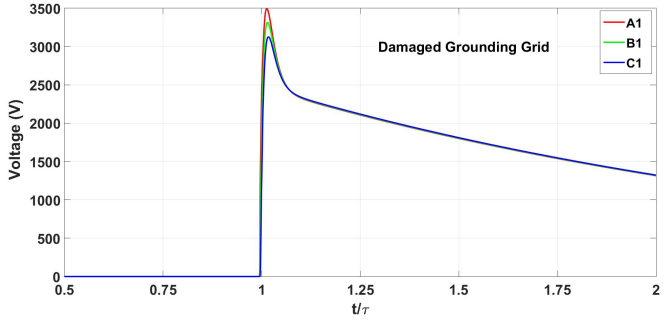

Figure 8. Voltages at the points A_1, B_1 and C_1 for a damaged grounding grid.

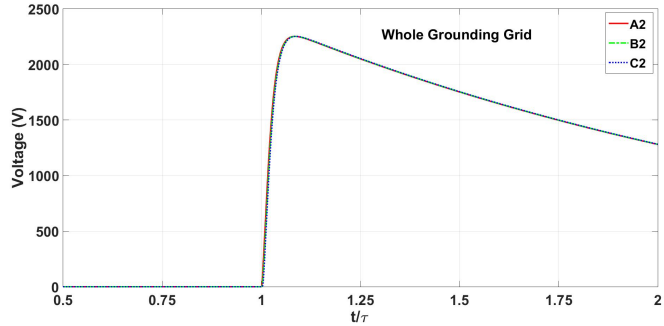

Figure 9. Voltages at the points A_2, B_2 and C_2 for a whole integrated grounding grid.

were computed at the points (nodes) (A_1, B_1, C_1), in the left side and at the (A_2, B_2, C_2), in right side, selected randomly as shown in Fig.5. The transient voltages at the points (A_1, B_1, C_1) for the whole (W) and damaged (D) grounding grid in the right part are depicted in Figs. 7 and 8, respectively.

One can note that voltages at points A_1, B_1 and C_1 present an expressive attenuation compared with the GPR peak (4.20 kV) as depicted in Fig. 7 and 8. This pronounced attenuation is due leakage conductance of the horizontal electrode through soil. The transient voltages at the (A_2, B_2, C_2) for the whole (W) and damaged (D) grounding grid in the left part of the grounding system are depicted in Figs. 9 and 10, respectively. In these cases, the voltages present practically the same peaks for a given scenario, characterized by high frequency content. The voltage peaks for at points (A_1, B_1, C_1) and (A_2, B_2, C_2) for whole and damage grounding grids (GG) are summarized in table 4.

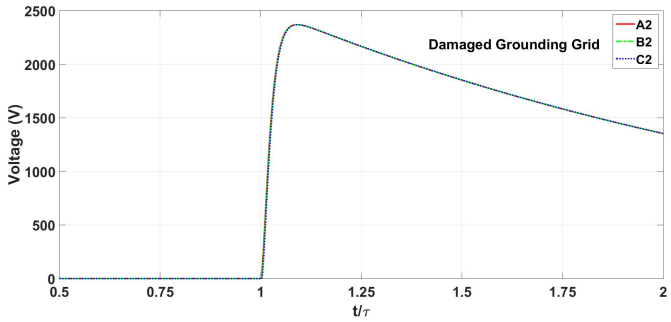

Figure 10. Voltages at the points A_2, B_2 and C_2 for a damaged grounding grid.

It can be noted that for a damaged GG, the voltage peaks at the two sides of the grounding system increase. When the nearest vertical rod of the injection current is damaged in the second grid, the voltages at the points (A_2, B_2, C_2) will increase of 120 V, compared with the whole GG. This elevation is more pronounced than the ones observed at the first GG, considering the whole and damaged cases. These higher values may compromise the safety of personnel in the vicinity and equipment concerning the step voltage inside the substation.

3.3 Transient Voltages with appended vertical rods

In an effort to decrease the transient voltages peaks observed in section 3.2, vertical rods are inserted at the border of the grounding grids. In this case, the new grounding grid topologies are depicted in Fig. 11.

The impulsive current was applied at the same condition of Fig.4. Figs. 12-14 display the voltages for each configuration of the vertical rods at points A_1, B_1, C_1 and A_2, B_2, C_2 for a damaged and a whole grounding grids.

It can be noted that transient peaks are reduced for all points when more rods are added in the grounding system. The curves obtained in the second grid are slower than the curves in the first grounding grid. This behaviour

Table 4. Voltage Peaks for the whole (W) and damaged (D) GG.

Voltage Peaks (kV)					
Point	W	D	Point	W	D
A_1	3.48	3.50	A_2	2.25	2.37
B_1	3.28	3.32	B_2	2.25	2.37
C_1	3.07	3.13	C_2	2.25	2.37

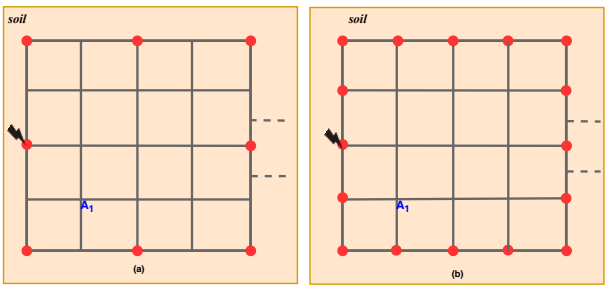

Figure 11. Alternative to reduce the node voltages in grids with: [(a) 8 rods and (b) 16 rods]

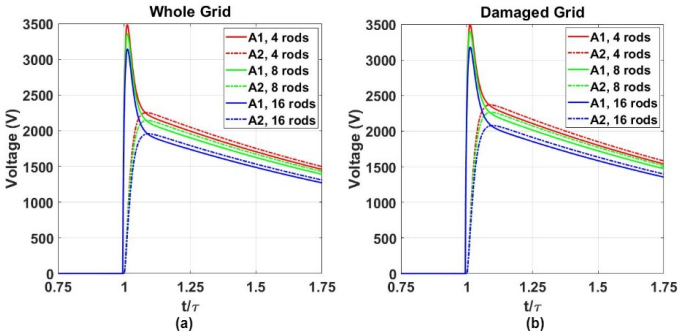

Figure 12. Voltages at A_1 and A_2 for the whole for 4, 8 and 16 vertical rods: [(a) and damaged (b) grounding grid].

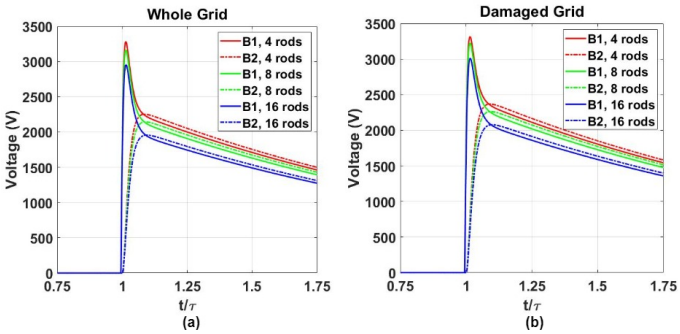

Figure 13. Voltages at B_1 and B_2 for the whole for 4, 8 and 16 vertical rods: [(a) and damaged (b) grounding grid].

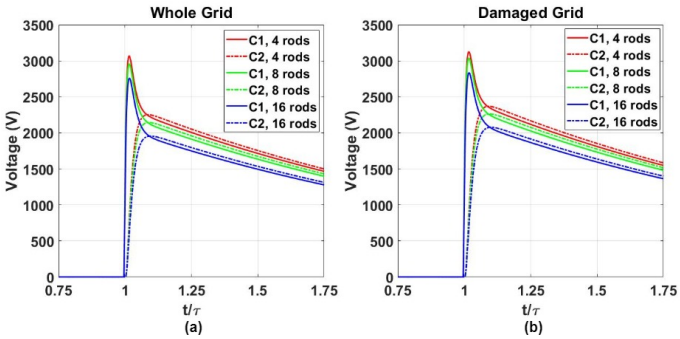

Figure 14. Voltages at C_1 and C_2 for 4, 8 and 16 vertical rods: [(a) and damaged (b) grounding grid].

happens because of the high change rate of impulsive currents flowing to the horizontal electrodes, where these inductances cause blocking effects in different sections of the grid.

For comparison, voltage peaks are shown in tables 5, 6 and 7.

Table 5. Voltage Peaks (kV) for different number of vertical rods at A_1 and A_2.

Voltage Peaks (kV) at A_1 and A_2				
	A_1		A_2	
	W	D	W	D
4 rods	3.48	3.50	2.25	2.37
8 rods	3.36	3.40	2.14	2.26
16 rods	3.15	3.18	1.96	2.08

Table 6. Voltage Peaks (kV) for different number of vertical rods at B_1 and B_2.

Voltage Peaks (kV) at B_1 and B_2				
	B_1		B_2	
	W	D	W	D
4 rods	3.28	3.32	2.25	2.37
8 rods	3.165	3.23	2.14	2.26
16 rods	2.96	3.01	1.96	2.08

Table 7. Voltage Peaks (kV) for different number of vertical rods at C_1 and C_2.

Voltage Peaks (kV) at C_1 and C_2				
	C_1		C_2	
	W	D	W	D
4 rods	3.07	3.13	2.25	2.37
8 rods	2.96	3.04	2.14	2.26
16 rods	2.76	2.84	1.96	2.08

Tables 5-7 show that the difference between the voltage peaks at point A_1 for the whole grounding grid witf 4 and 16 rods reaches 300 V. For the damaged GG, the difference is approximately 320 V when compared with the simulation results between 4 and 16 rods. These differences are just related to node voltages and not between two nodes on the grounding grids.

4. CONCLUSIONS

The results reveal the value of the transient voltages to be quite large (of kilovolts), representing a possible threat to the people and equipment in the affected area. If the grounding grid has any defects, these transient voltages are calculated to be even larger. With these facts in mind, the addition of extra vertical rods can be an effective solution to reduce these amplitudes across the grounding grids, since this method was able to lower the voltage peaks of 10% approximately between the configuration with 4 and 16 rods in all the grids. Furthermore, the inductance is also a very important parameter for the grounding grid model. As observed at the points A_2, B_2 and C_2 the voltage have a slower change rate in comparison with points A_1, B_1 and C_1, due to the larger inductance between the points of the secondary and the first grid.

ACKNOWLEDGMENTS

We thank to the High Voltage Laboratory group (LAT) at School of Electrical and Computer Engineering (FEEC) at University of Campinas.

REFERENCES

Ala, G., Favuzza, S., Francomano, E., Giglia, G., and Zizzo, G. (2018). On the distribution of lightning current among interconnected grounding systems in medium voltage grids. *Energies*, 11(4), 771.

Cecconi, V., Matranga, A., and Ragusa, A. (2005). New circuital models of grounding systems and pds for emi analysis during a lightning strike. In *31st Annual Conference of IEEE Industrial Electronics Society, 2005. IECON 2005.*, 6 pp.–.

Chikarov, Y., Lie, T., and Nair, N. (2014). A new monitoring technique for the grounding grids. *Open Engineering*, 4(3), 293–302.

Farkoush, S.G., Wadood, A., Khurshaid, T., Kim, C.H., Irfan, M., and Rhee, S.B. (2019). Reducing the effect of lightning on step and touch voltages in a grounding grid using a nature-inspired genetic algorithm with atp-emtp. *IEEE Access*, 7, 81903–81910.

Grcev, L. and Grceva, S. (2009). On hf circuit models of horizontal grounding electrodes. *IEEE Transactions on Electromagnetic Compatibility*, 51(3), 873–875. doi: 10.1109/TEMC.2009.2023330.

Grcev, L. and Popov, M. (2005). On high-frequency circuit equivalents of a vertical ground rod. *IEEE Transactions on Power Delivery*, 20(2), 1598–1603. doi: 10.1109/TPWRD.2004.838460.

Grcev, L.D. and Heimbach, M. (1997). Frequency dependent and transient characteristics of substation grounding systems. *IEEE Transactions on Power Delivery*, 12(1), 172–178.

Han, X., Lu, Y., Xia, C., Yu, J., Huang, Y., Zhou, W., Xu, B., and Li, H. (2011). Simulation research on impulse characteristics of horizontal grounding conductor. In *2011 IEEE Power Engineering and Automation Conference*, volume 2, 31–35. IEEE.

Harrat, B., Nekhoul, B., Kerroum, K., and Drissi, K.E.K. (2011). A simplified approach to modeling the interaction between grounding grid and lightning stroke. *annals of telecommunications-annales des télécommunications*, 66(11-12), 603–615.

Hassan, A.M., Abdallah, E.N., and Abbasy, N.H. (2012). Design and simulation of interconnected a.c substation grounding grid in oil gas industries. In *2012 Japan-Egypt Conference on Electronics, Communications and Computers*, 188–193. doi:10.1109/JEC-ECC.2012.6186981.

Jardines, A., Guardado, J., Torres, J., Chávez, J., and Hernández, M. (2014). A multiconductor transmission line model for grounding grids. *International Journal of Electrical Power & Energy Systems*, 60, 24–33.

Otero, A.F., Cidras, J., and Garrido, C. (2000). Geometrical considerations in the frequency behaviour of grounding systems. In *Ninth International Conference on Harmonics and Quality of Power. Proceedings (Cat. No.00EX441)*, volume 1, 274–277 vol.1. doi:10.1109/ICHQP.2000.897039.

Ramirez, A., Gomez, P., Moreno, P., and Gutierrez, A. (2004). Frequency domain analysis of electromagnetic transients through the numerical laplace transforms. In *IEEE Power Engineering Society General Meeting, 2004.*, 1136–1139. IEEE.

Salam, M.A. and Rahman, Q.M. (2016). Grounding system parameters and expression of ground resistance. In *Power Systems Grounding*, 154–201. Springer.

Sheshyekani, K., Hesamedin Sadeghi, S.H., Moini, R., Rachidi, F., and Paolone, M. (2009). Analysis of transmission lines with arrester termination, considering the frequency-dependence of grounding systems. *IEEE Transactions on Electromagnetic Compatibility*, 51(4), 986–994. doi:10.1109/TEMC.2009.2029863.

Wang, X., Fu, Z., Wang, Y., Liu, R., and Chen, L. (2019). A non-destructive testing method for fault detection of substation grounding grids. *Sensors*, 19(9), 2046.